Vol 18 No 12, December 2009
1674-1056/2009/18(12)/5406-08

Chinese Physics B

© 2009 Chin. Phys. Soc.
and IOP Publishing Ltd

Mitigation and prediction of disruption on the HL-2A Tokamak*

Zheng Yong-Zhen(郑永真)†, Qiu Ying(邱 银), Zhang Peng(张 鹏), Huang Yuan(黄 渊), Cui Zheng-Ying(崔正英), Sun Ping(孙 平), and Yang Qing-Wei(杨青巍)

Southwestern Institute of Physics, Chengdu 610041, *China*

(Received 26 June 2008; revised manuscript received 6 March 2009)

Injection of high-Z impurities into plasma has been proved to be able to reduce the localized thermal load and mechanical forces on the in-vessel components and the vacuum vessel, caused by disruptions in Tokamaks. An advanced prediction and mitigation system of disruption is implemented in HL-2A to safely shut down plasmas by using the laser ablation of high-Z impurities with a perturbation real-time measuring and processing system. The injection is usually triggered by the amplitude and frequency of the MHD perturbation field which is detected with a Mirnov coil and leads to the onset of a mitigated disruption within a few milliseconds. It could be a simple and potential approach to significantly reducing the plasma thermal energy and magnetic energy before a disruption, thereby achieving safe plasma termination. The plasma response to impurity injection, a mechanism for improving plasma thermal and current quench in major disruptions, the design of the disruption prediction warner, and an evaluation of the mitigation success rate are discussed in the present paper.

Keywords: disruption, current quench, electro-magnetic load, thermal load, mitigation and prediction of disruption

PACC: 5255, 5255G, 5255V, 6180B

1. Introduction

Plasma disruptions have three major negative effects on a Tokamak. They cause 1) localized deposition of thermal energy on the plasma facing components; 2) generation of runaway electrons in the torus and 3) large mechanical forces acting on the electrically conducting structures. Nevertheless, these effects can be significantly reduced by the injection of a high-Z impurity before the thermal quench occurs. Therefore experiments on disruption mitigation are carried out nowadays on all large Tokamaks to investigate the influence of the injected impurities on the development of the disruption. The species of high-Z impurity, the rate of injection and the injected quantities differ considerably, depending on the type of high-Z impurity injection system available and the volume of the vessel. In this framework, experiments have been conducted on HL-2A for years[1] and the injection of Ti, Al using laser ablation for the plasma to safely shut down has been employed. The injection is usually triggered with an MHD perturbation field detected by a Mirnov coil and leads to the onset of a mitigated disruption within a few milliseconds.

The optimal disruption mitigation requires that all three deleterious effects of disruptions are reduced below acceptable engineering margins. In order to reduce the localized heat deposition during the thermal quench of the disruption, the injected impurity must store ionization energy and release most of the thermal energy of the plasma before magnetic instabilities can cause a thermal quench. In order to do this, the injected impurity must

(i) penetrate as neutral into the plasma;

(ii) penetrate fast, i.e. before the thermal quench sets in;

(iii) radiate as much as possible. The specific radiation efficiency $f_{\rm I}$, and therefore the radiated power $P_{\rm rad} = f_{\rm I} n_{\rm e} n_{\rm I}$, increases from low to high Z ($n_{\rm e}$ and $n_{\rm I}$ indicate the electron and impurity densities respectively).

Mitigation of both halo currents and diverter thermal deposition ultimately depends on the ability to convert a significant fraction of the total plasma stored energy, $W_{\rm tot} = W_{\rm th} + W_{\rm mag}$, into benign radiation on a timescale faster than an unmitigated disruption ($W_{\rm th}$ and $W_{\rm mag}$ denote the plasma thermal energy and the magnetic energy respectively). Therefore HL-2A provides a very challenging test of the ability to convert stored energy into radiation.

*Project supported by the National Natural Science Foundation of China (Grant No 10475023).

†Corresponding author. E-mail: yongzhen.zheng@gmail.com

A high-Z impurity (KCl) pellet injection has been used in such an experiment on T-10[2] and noble gas jet injection has been used for disruption mitigation on DIII-D,[3] ASDEX-U.[4] In the present paper it is reported that preliminary experiments are performed in HL-2A and HL-1M using the injection of Ti or Al by laser ablation to investigate this approach.

The modelling of the complex phenomena following impurity plasma interaction and the requirements for the application of mitigation techniques in ITER are not discussed in the present paper.

2. Experiments on impurity injection using laser ablation

2.1. Experimental layout

The main idea of the experiments is to obtain a resistive highly-radiating plasma formed prior to the thermal quench and to increase the efficiency of plasma cooling due to high-Z impurity radiation. The radiation source is created by the laser ablation of Ti or Al. A laser beam with an energy output of 2–5 J and a pulse duration of 30 ns is focused on metal films with 10 μm thickness and produces a burst of metal gas, which moves towards the plasma centre. Figure 1 shows the real-time control system using the laser ablation of impurities. The laser spot with a diameter of 1–3 mm contains a few 10^{19} atoms of metalline element. When those metallic atoms move towards the plasma edge and the confinement region, they experience the following processes: ionization, collision and diffusion. If the ions at various ionization levels of injected impurities are wholly distributed in the core confinement region, the ion density well occupies 0.5%–2% of the electron density in the plasma central region ($r/a < 1/5$),[5] which can be demonstrated by absolute measurements from the VUV (vacuum ultra violet) spectrometer with the impurity transport code SITCODE simulation.[5] In fact, only a fraction of such ions can reach the centre. The target chamber is attached to the midsection of the vessel, and the injection point is approximately 1.1 m from the plasma boundary. The injected neutral particles have a measured energy of a few eV and reach the plasma boundary in less than 0.5 ms. The neutral atoms are ionized on the plasma edge and spread out rapidly along the field lines. At the same time, because of collisions or turbulence, the ions move slowly and radially inwards typically at speeds of 5–10 m/s that are measured with a CCD camera. The penetration of the impurities into the plasma is observed by using two soft x-ray imaging cameras and a CCD camera. The penetration radius is about 25 cm measured by the CCD camera, or evaluated from the ionization levels of injected impurities (Al^{10+}, Al^{11+} and Al^{12+}) measured with a VUV spectrometer.[6] The impurity particles normally travel inward half of the minor radius and create a maximum impurity deposition there.

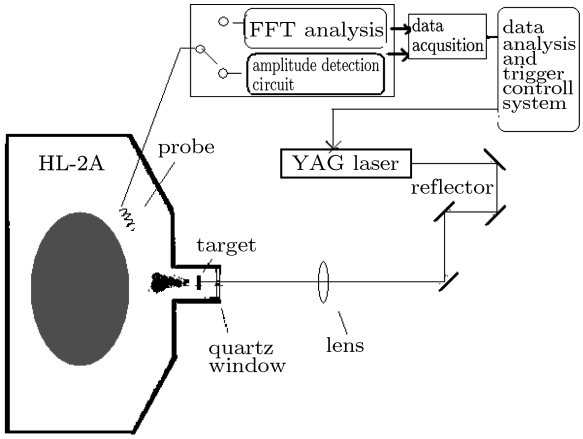


Fig.1. Real-time control system for disruption mitigation using laser ablation of impurities.

The plasma behaviour varies with the quantity of injected impurity and the plasma density. The injection of a small fraction ($< 0.01\%$) of the electron density causes slight perturbations of $\Delta n_e/n_e \sim 0.05$ and $-\Delta T_e/T_e \sim 0.2$. Such plasma parameters as $T(r,t)$, loop voltage $V_l(t)$ are relaxed in 20–40 ms to new steady-state levels which are close to those prior to the injection. No changes in $m = 2$ MHD (magneto-hydrodynamic model) activity or in the 'hard x-ray' signal (HXR emission with energy more than 3 MeV) are observed.

2.2. Plasma behaviour after injection of impurity

The experimental sequence of events is shown in Fig.2. When the injected impurity enters and contacts the plasma surface, the edge temperature suddenly drops off and a loss of thermal energy occurs. The injected impurity ionizes and undergoes mass toroidal deposition and then achieves toroidal–poloidal symmetrization of the electron density, an impurity plasma forms and the current starts to decay. Perturbations in the poloidal and radial fields appear and grow but only up to a moderate amplitude. At

this stage, the total power radiated significantly increases (see Fig.2(f), in which signals are measured by a barometer). A cooling front begins to propagate into the plasma, and when it reaches $q = 2$ radius, the growth of a mode with $m = 2$ and $n = 1$ is triggered. This is observed experimentally (Fig.2(d)). The cooling front is due to the growth of MHD instabilities. Then significant temperature perturbation in the ambient plasma reaches $(-\Delta T_e/T_e)$ ~0.7–0.9, $(-\Delta n_e/n_e$ ~0.25–0.5) due to the deposition of impurities. The central temperature T_{e_0} continues to rapidly collapse into the $q = 1$ radius, leading to a large growth of instability for the $m = 1$ and $n = 1$ mode (Fig.2(e)). This results in large ergodic regions and the destruction of flux surfaces, loss of core confinement, and eventual current quench (Fig.2(a)). When T_{e_0} rapidly collapses, a significant reduction in plasma energy content $\Delta W/W$ is observed; the reduction is measured to be about 80% of its maximum value in shot #03875. As a result of plasma cooling the vertical position control is switched off, but the vertical position is essentially unchanged. With the loop voltage further increasing, the electron temperature reaches its minimal value.

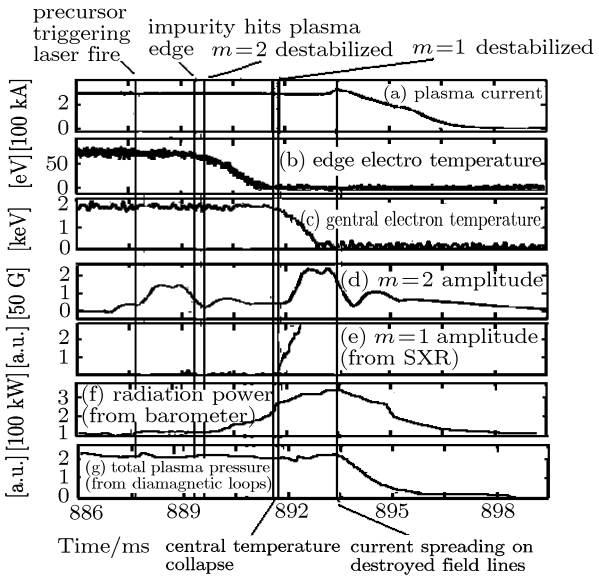


Fig.2. The experimental sequence of events, and measurements of (a) plasma current, (b) edge electron temperature, (c) central electron temperature, (d) m=2 amplitude of poloidal magnetic field perturbations, (e) m=1 amplitude, (f) radiation power and (g) total plasma pressure as a function of time for an impurity injected shot in HL-2A.

When current decay ends, a very small non-thermal current appears and the total current increases only by 10 kA that is above an extrapolated value from the resistive decay. An extended period of negative loop voltage appears. The vertical position then returns to the vicinity of the vessel centre and the discharge terminates on the inner wall. The electron energy content is not restored after the disruption.

2.3. Temperature, SXR and MHD activity

Afterwards the whole temperature profile collapses within 0.1 ms as in a natural thermal quench. The SXR diagnostic shows similar behaviour for the line integrated emission. The injection of impurities triggers the onset of large MHD activity.

The electron temperature drop-off is measured by using an ECE (electron cyclotron emission receiver) as shown in Fig.2(c). The drop-off in T_e at the moment of disruption is due to not only the enhancement of transport across the minor radius but also the radiation cooling. The magnitude of the temperature drop-off is roughly proportional to the number of electrons deposited. The loss is also indicated by the plasma β in the equilibrium analysis reducing to the vicinity of zero and the resulting horizontal shift of the plasma. The loss of total plasma pressure measured by diamagnetic loops is observed as shown in Fig.2(g).

Soft x-ray emission during the injection is carried out in two stages, and the measurements are shown in Fig.3. After the ablation of the injected impurity, the radiation profile builds up at minor radius immediately, with no increase in radiation from

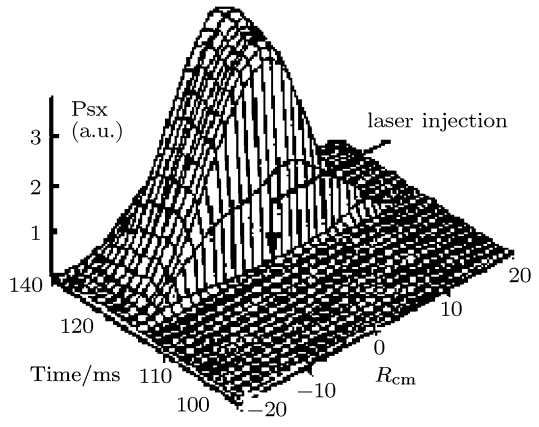


Fig.3. The soft x-ray emission during the injection continues in two stages.

the centre. In the central region no sawtooth crash occurs.[7] Then it takes 1–2 ms for the radiation profile to become peaked on the axis.

Before disruption, the amplitudes of mode $m = 2$ ($q = 2$) and later mode $m = 3$ ($q = 3/2$) increase and are measured using the MHD Fourier technique. We simulate the evolution of the current density profile $j(r, t)$ after impurity injection by using the diffusion equation for a poloidal magnetic field. The neoclassical plasma conductivity is calculated from the experimental profiles $T_{\rm e}(r, t)$. The simulated $j(r, t)$ profiles then serve as the input data for the code to calculate stability and parameters of magnetic islands.[8] The simulation results show that all modes with the poloidal number $m > 4$ are stable at all times while the $m = 2$, 3, 4 modes are still developing. The external boundary position of the $m = 3$ ($q = 3/2$)$r_{3/2}^{\rm ext}(t)$ island and the internal boundary position of the $m = 2$ ($q = 2$)$r_2^{\rm int}(t)$ island overlap. The central temperature $T_{\rm e_o}$ continues to rapidly collapse into the $q = 1$ radius, leading to a large $m = 1$, $n = 1$ mode activity. It is seen that the disruption occurs at the moment when the $q = 2$ and $q = 3/2$ islands are intercepted and the $m = 1$ mode is excited. This implies an appreciable influence of the $j(r, t)$ evolution on the disruption development.

2.4. Runaway electrons, mechanical loads and radiated energy

Runaway electrons (RE) are rare events and appear only in discharges with target density $n_{\rm e} < 1 \times 10^{19}$ m^{-3} and $B_{\rm t} > 2$ T in HL-2A. A steady increase in the hard x-ray rate is rarely observed. The increase is presumed to reflect a gradual buildup of energetic electrons during the initial current decay. But the current carried by runaway electrons is very low and so increases only by 10 kA that is above an extrapolated value from the resistive decay. The suppression of the runaway electron (RE) generation requires a slow current quench for the reduction of the toroidal electric field below the critical electric field, $E_{\rm c} \propto n_{\rm e}/T_{\rm e}$, and the increase of this threshold through the density. But the generation of runaway electrons can also be reduced easily by using an intensive massive neon or helium puff.[3]

The larger mechanical forces acting on the vessel during natural disruptions are due to larger induced currents in the halo region. The mechanical forces obviously induce radial vessel displacements. The measurements estimate that currents are reduced by a factor of 1.5–3, with the injection of impurity used. The radial vessel displacements at the top and bottom of the vessel measured at 4-th toroidal locations on HL-2A with an accurate vibration measuring instrument (precision: 0.1 mm) show that the magnitude of the displacement produced by laser ablation of the high-Z impurities which can cause current termination is small and almost symmetric, indicating that a little influence of the laser ablation of impurities takes place. Although the vessel has ripple sections, the received power is symmetric, and, as a whole, the influence of displacement is less. The vacuum vessel displacements indicate the severity of the force which is toroidally symmetric during a disruption as shown in Fig.4.

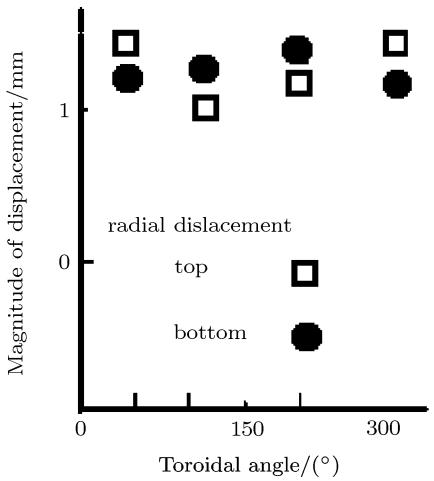


Fig.4. Radial vessel displacement.

The radiation power ($P_{\rm rad}$) as a function of time for an impurity injection shot is shown in Fig.2(f). Both thermal energy and magnetic energy appear to be dissipated largely by radiation. The larger amount of radiated plasma energy after mitigation is partly due to the larger energy of the plasma at the time of mitigation and partly results from the effect of the injected impurity.

3. Disruption forecasting

Disruption prediction is carried out in the HL-2A Tokamak by using an MHD perturbation real-time measuring and processing system. The architecture of the disruption prediction system is shown in Fig.5, including an MHD perturbation detector, real-time data measuring, a disruption precursor acquisition and processing system, data analysis and a laser ablation sys-

tem of high-Z impurities.

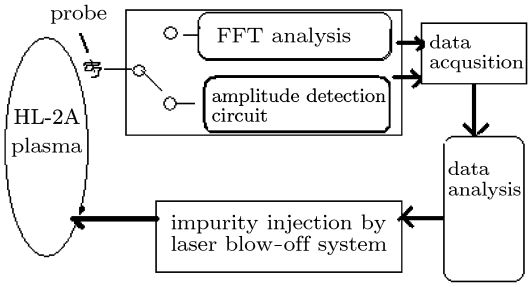


Fig.5. MHD real-time measuring and processing system to predict major disruptions on the HL-2A Tokamak.

3.1. Principle of MHD activity detection

When MHD activity increases, the characteristics of the amplitude and frequency of the MHD perturbation field detected by the Mirnov coil are shown in Fig.5. The beginning of the signal has no MHD activity. After MHD perturbation has grown, the amplitudes have larger changes and always are more than 1.0 V. Both segments t_1 = 440–441 ms (without MHD activity) and t_2 = 550–551 ms (with MHD activity) are selected to process a frequency spectrum analysis with fast Fourier techniques (FFT) and to obtain the power spectrum shown in Fig.6. We find that the power components of the frequency sect (1–7 Hz) occupy larger components during segments t_2 = 550–551 ms. But the power spectrum is distributed at an average level during segments t_1 = 440–441 ms. Finally, the amplitudes increase, but the frequency decreases, followed by a long duration of locked mode, then a larger disruption discharge occurs.

The MHD features of disruption discharge are 1) amplitudes > 1.0 V and 2) range of frequency: 1–7 Hz. The real-time data measuring, acquisition and processing of MHD perturbation are performed using two methods: checking and measuring the amplitude and frequency. The principle of the former is to set an amplitude threshold V_t and to compare the sampling amplitude values with V_t: when most of the sampling amplitude values are greater than V_t in the measurement cycle, the discharge can be considered to be the occurrence of a disruption precursor. The principle of the latter is to process a frequency spectrum analysis on signals in the measurement cycle and then to compute the ratio of the power component of the frequency sect (1–7 Hz) to the entire power spectrum. If the ratio is larger than the threshold value P_t, the discharge will be considered to be the occurrence of a disruption precursor.

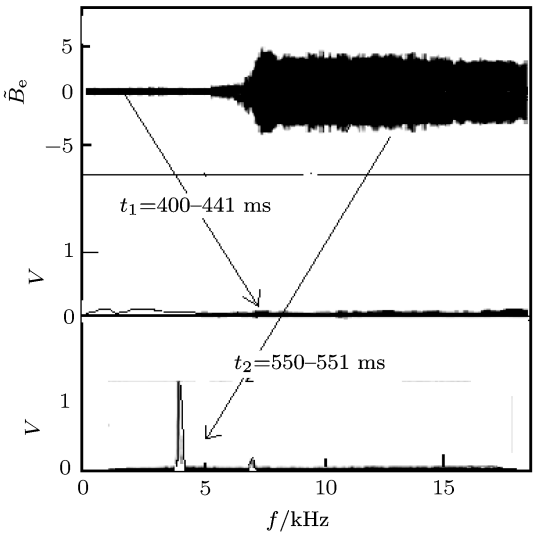


Fig.6. Amplitude and frequency characteristics of MHD.

3.2. Requirement of system design

The disruption precursor real-time acquisition and processing system must have three characteristics:

Real time: When the signals shows a disruption precursor, the checking and processing system can send out a control signal to trigger the laser ablation system. Ordinarily the response time is on the order of ms. Checking, processing and sending out the trigger signal must be completed in 1 ms.

Parallel: In experiment both the data acquisition and the data processing must be performed in parallel. The data acquisition card must include a double-buffer and operate with the DMA model.

High sampling rate: In the MHD acquisition and processing system, the checking cycle period is set to 1 ms. A checking cycle includes 1000 sampling points. The sampling rate of the acquisition card is 1–2 MHz.

We adopt DAQ/PXI-2010[9] as an acquisition card; this is an advanced data acquisition card based on 32-bit PCI architecture. Using high performance design and state-of-the-art technology the factory makes this card ideal for data logging signal analysis applications in process control, etc. The card includes 4-channel simultaneous differential analog inputs, 14-bit analog input resolution with a sampling rate up to 2 MS/s, total 8 K samples A/D FIFO and a double-buffer. This card satisfies the requirements for system design completely.

3.3. System implementation

3.3.1. General configuration

We implement the MHD real-time measuring and processing system by means of amplitude and frequency separately. The architecture of the general configuration is shown in Fig.5. The original signals from the magnetic field coil via photoelectric isolation are routed to the both-switch. If the system intercepts the trigger signal of discharges, then the original signals input to the acquisition system. It immediately processes the data acquired. The acquisition card transports the data acquired alternately to two buffers. While the data is transported to buffer 1 in the acquisition card, the system reads data from buffer 2 and processes and analyses the data in order to engender the trigger signal via the I/O port to the laser ablation system. If the trigger signal received is at a high electric level, this discharge will denote the occurrence of a disruption precursor, and then the system immediately triggers the laser. We adopt double buffer acquisition so that the system can ensure continuous acquisition while at the same time it performs real-time measuring, processes data and sends the trigger control signal.

3.3.2. MHD amplitude means

In MHD frequency means, a 'swing containing line' diode cymoscope is adopted as an amplitude detecting circuit, and the amplitude oscillation can be obtained after signal detection. At first, we denote the relevant parameters of MHD detection as follows: Y: swing threshold, Y_Num: number of sampling points for amplitude swing more than Y in a cycle, Total_Num: total number of sampling points, Ratio: Y_Num/Total_Num, and Max_Ratio: presetting maximum ratio. If Ratio>Max_Ratio, the discharge will be considered to be the occurrence of a disruption precursor, otherwise no precursor occurs.

3.3.3. MHD frequency means

In MHD frequency means, we must perform a frequency spectrum analysis with FFT arithmetic. All acquired time region signals are transformed into frequency region signals. In the FFT arithmetic the length of the input data sequence must satisfy the condition $N = 2^L$. Setting $N = 2^{10} = 1024$, the system collects 1000 signal points.

Pending the check data sequence $x(j)$, where j=1, 2, 3, ... , 1023, the system transits the FFT arithmetic and turns into a plural sequence team: $y(j) = y_\mathrm{real}(j) + y_\mathrm{image}(j) \times i$, where j=1, 2, 3, ... , 1023, $|y(j)|$ denotes the power component at the j point. The MHD signals come to exhibit definite frequency character and the frequency range is 1–7 kHz. Performing an integration of $y(j)$ over the frequency range (1–7) kHz, the integral results are denoted as A, then the integral results over all frequency ranges are represented by B. Calculating $P_{\mathrm{ratio}} = A/B$, we can obtain the power component of frequency and then, based on the value of P_{ratio}, judge whether a disruption precursor has appeared or not.[9]

4. Success rates of disruption mitigation

A further requirement for any mitigation method is the low contamination of subsequent plasma discharges; we emphasize not only increasing the success ratio of disruption prediction but also reducing the distortion ratio in order to avoid polluting the equipment. Therefore we must enhance the effectiveness of the mitigation system, since the effectiveness of such a mitigation system strongly depends on the success ratio of disruption prediction and the time delay of mitigation.

4.1. Success ratio of disruption prediction

In amplitude means, the total number of discharges is 35. Of these, 12 shots indicate the occurrence of the disruption. 10 of the 12 shots are successfully predicted to be disruptive discharge. So, the success ratio of disruption prediction is 10/12=83%. In frequency means, the total number of discharges is 40, of which 10 shots show the presence of disruption. 8 of the 10 shots are successfully predicted to be disruptive discharge. Therefore, the success ratio of disruption prediction is 8/10=80%.

The prediction is quite successful. The advantage of these means is their high sensitivity and their disadvantage is the difficulty in confirming accurately the frequency range of MHD activity. However, here the prediction is implemented only for large MHD perturbation activity, not for various types of disruptions, e.g. density limit, locked mode, high internal induc-

tance disruptions. An advanced neural network system for various types of disruptions will be carried out in the near future.

4.2. Time delay of mitigation

The time delay of the mitigation system is the time delay between the laser trigger and the start of the current quench. The current quench after impurity injection can begin with the typical current hump, indicating a fast redistribution of the current profile or the current rolling over towards its decay without any hump. The majority of the induced current quenches have a reduced or no current hump. For discharges with a clear current hump we define a delay time $\Delta t_{\rm delay}$. This time interval is the sum of the impurity flying time ($\Delta t_{\rm fly}$) from the laser opening to the plasma edge (of approx 0.2 ms), the cooling time ($\Delta t_{\rm cool}$) and the inherent time delay ($\Delta t_{\rm in}$) due to the pumping time of the laser for laser action,[1] the travelling time of the gas through the gas delivery pipe for the gas jet system[3] or the time for pellet quick freezing for pellet injection.[2] $\Delta t_{\rm cool}$ is observed to vary from zero to 2 ms mostly depending on the thermal energy of the impurity plasma.

Here, mitigation success rates are defined as the ratio of the number of disruptive discharges which are successfully mitigated to the total number of disruptive discharges. This assessment can be performed by using the sophisticated disruption prediction methods developed recently, such as the above-mentioned MHD perturbation real-time processing and analysing system or the neural network system,[10] applied to the possible mitigation scenarios. The mitigation success rate is strongly related to the hardware response time, which is closely linked to the response time of the MHD perturbation real-time measuring and processing system from the occurrence of a disruption precursor to the laser opening, and the plasma response time before the occurrence of the radiation collapse after the impurity reaches the plasma edge. The quench time seems to be strongly dependent on the extent of the incoming particle penetration.

A comparison between the values of $\Delta t_{\rm delay}$ obtained from three different mitigation techniques, i.e. laser ablation, gas jet, and pellet injection, which can be used to estimate the time delay of migration from the experimental data available from HL-2A,[1] DIII-D,[3] ASDEX-U[4] and T-10,[2] is made and the results are summarized in Table 1. This implies that if the time delay of mitigation $\Delta t_{\rm delay}$, i.e. the time interval from the occurrence of a disruption precursor to disruption, is only less than the plasma disruption response time $\tau_{\rm d}$, the disruption mitigations can succeed. Of the mitigation techniques proposed, the laser ablation technique seems to be the most promising. This technique provides less mitigation time delay and enhances the success ratio of prediction to mitigation.

Table 1. Comparison between the values of time delay of mitigation $\Delta t_{\rm delay}$ obtained for three different mitigation methods.

	laser ablation	gas jet injection	pellet injection
$\Delta t_{\rm delay}$ the time delay of mitigation	2.5 ms	5–10 ms	10 ms
$\Delta t_{\rm fly}$ the impurity flying time	0.2 ms	2 ms	0.1 ms
$\Delta t_{\rm cool}$ the cooling time	2 ms	2–6 ms	$<$ 2 ms
$\Delta t_{\rm in}$ the inherent time delay	0.2 ms	6 ms	8 ms

5. Conclusions

(I) An advanced prediction and mitigation system is developed on the HL-2A Tokamak to safely shut down plasmas by using the laser ablation of high-Z impurities, with MHD perturbation real-time measuring and processing. A better effect in the project for mitigating disruption discharges is anticipated.

(II) The injection of high-Z impurity into the HL-2A plasma shows the possibility of fast ($\sim$2 ms) plasma cooling and loss of about 80% of the energy before the disruption occurs.

(III) High-Z impurities are chosen, with the purpose of enhancing the $Z_{\rm eff}$ in the plasma centre at high $T_{\rm e}$, and producing a large electron density perturbation, both of which can provide a strong radiation source and reduce the background electron temperature immediately below 0.1 keV by dilution. The impurity content in shots following fast plasma shut-down may accumulate and influence the performance of subsequent discharges.

Therefore the injection of impurities should be limited to dangerous disruptions and its efficiency optimized. A search for an optimal configuration for the type of high-Z impurity, the rate of injection and the injected quantities, which seem to compromise deep and fast penetrations, high radiation cooling and low residual plasma contamination, will be carried out in the near future.

(IV) The experimental results indicate that a resistive highly-radiating plasma, formed prior to the thermal quench, could dissipate both the thermal and magnetic energies with little MHD activity present and minimize the risk of local deposition.

(V) The response time of the MHD real-time measuring and processing system on the HL-2A Tokamak completely satisfies the experimental requirements. Of the mitigation techniques proposed up to now, the laser ablation technique seems to be the most promising. This technique provides less mitigation time delay and enhances the success ratio of prediction to mitigation.

References

[1] Zheng Y Z, Feng X Y, Guo G C, Xu D M and Zheng Y J 2006 *Chin. Phys.* **15** 1009

[2] Kuteev B V, Sergeev V Yu and Sudo S N 1995 *Nucl. Fusion* **35** 397

[3] Hollmann E M, Jernigan T C, Whyte D G, Austin B D, Brennan D P, Strait E J and West W P 2005 *Nucl. Fusion* **45** 1046

[4] Pautasso G and the ASDEX Upgrade Team 2006 *Proc. 21th IAEA FEC* Chengdu EX/P8-7

[5] Zheng Y, Cao Z and Li W 2002 *Nuclear Fusion and Plasma Physics* **22** 17 (in Chinese)

[6] Luo C X, Li K F and Wang Q M 1991 *Research Using Small Tokomaks* Presented at IAEA Technical Committee Meeting 82

[7] Dong G F, Shi B R, Li W and Luo J L 2004 *Chin. Phys.* **13** 379

[8] Chudnovskij V Yu 1984 *IAEA-R-887/6*

[9] Wang H, Luo J N, Li Z Y and Huang Q C 2005 *Nuclear Techniques* **28** 10 (in Chinese)

[10] Yoshino R 2005 *Nucl. Fusion* **45** 1232